Supplementary Information

$IrAu_{12}$ superatom modified by chiral diphosphines: Doping-induced enhancement of chiroptical activity

Haru Hirai,[1] Takuya Nakashima,*[2,3] Shinjiro Takano,[1] Yukatsu Shichibu,[4,5] Katsuaki Konishi,*[4,5] Tsuyoshi Kawai,[2] and Tatsuya Tsukuda*[1]

[1]*Department of Chemistry, Graduate School of Science, The University of Tokyo, Hongo 7-3-1, Bunkyo-Ku, Tokyo 113-0033, Japan*
[2]*Division of Materials Science, Nara Institute of Science and Technology (NAIST), Takayama 8916-5, Ikoma, Nara 630-0192, Japan.*
[3]*Department of Chemistry, Graduate School of Science, Osaka Metropolitan University, Sugimoto 3-3-138, Sumiyoshi-ku, Osaka 558-8585, Japan.*
[4]*Graduate School of Science, Hokkaido University, North 10 West 5, Sapporo 060-0810, Japan*
[5]*Faculty of Environmental Earth Science Hokkaido University, North 10 West 5, Sapporo 060-0810, Japan*

1. Methods

Chemicals

The solvents, 1,5-cyclooctadiene (COD), 2,2′-thiodiethanol, dimethyl sulfide (SMe_2), chloroauric acid tetrahydrate ($HAuCl_4{\cdot}4H_2O$), sodium borohydride ($NaBH_4$), sodium hexafluorophosphate ($NaPF_6$), 12 M hydrochloric acid (HCl aq), and activated alumina (~75 μm) for column chromatography were purchased from Fujifilm Wako Pure Chemical Industries. 1,2-Bis(diphenylphosphino)ethane (dppe), and ceric ammonium nitrate (CAN) were purchased from Tokyo Chemical Industry. (*R*,*R*)-1,2-bis[(2-methoxyphenyl)phenylphosphino]ethane ((*R*,*R*)-DIPAMP) and (*S*,*S*)-1,2-bis[(2-methoxyphenyl)phenylphosphino]ethane ((*S*,*S*)-DIPAMP) were purchased from Sigma-Aldrich. Iridium chloride trihydrate ($IrCl_3{\cdot}3H_2O$) was purchased from Tanaka Precious Metals. The water used was Milli-Q grade (>18 MΩ). All commercially available reagents were used as received. $(AuCl)_2$(dppe) was synthesized from $HAuCl_4{\cdot}4H_2O$ and dppe by using 2,2'-thiodiethanol.[1] $AuCl(SMe_2)$ was synthesized from $HAuCl_4{\cdot}4H_2O$ and SMe_2.[2] $(AuCl)_2$((*R*,*R*)-DIPAMP) and $(AuCl)_2$((*S*,*S*)-DIPAMP) were synthesized from $AuCl(SMe_2)$ with (*R*,*R*)-DIPAMP and (*S*,*S*)-DIPAMP, respectively.[3] $[Ir(COD)Cl]_2$ was synthesized from $IrCl_3{\cdot}3H_2O$ and COD.[4] $[Au_{13}(dppe)_5Cl_2](PF_6)_3$ (**Au_{13}-dppe**·$(PF_6)_3$) was synthesized from $(AuCl)_2$(dppe).[5] $[Au_{13}((R,R)\text{-DIPAMP})_5Cl_2](PF_6)_3$ (**Au_{13}-R**·$(PF_6)_3$) and $[Au_{13}((R,R)\text{-DIPAMP})_5Cl_2](PF_6)_3$ (**Au_{13}-S**·$(PF_6)_3$) were synthesized from $(AuCl)_2$((*R*,*R*)-DIPAMP) and $(AuCl)_2$((*S*,*S*)-DIPAMP), respectively.[3] $[IrAu_{12}(dppe)_5Cl_2](PF_6)$ (**$IrAu_{12}$-dppe**·(PF_6)) was synthesized from $(AuCl)_2$(dppe) and $[Ir(COD)Cl]_2$.[6]

General

Positive-mode electrospray ionization (ESI) mass spectra were recorded on a Bruker

compact ESI-Q-TOF mass spectrometer. A sample solution in acetonitrile was infused at a flow rate of 5 μL/min using a syringe pump. The measurement parameters are as follows: end plate offset voltage: −500 V; capillary voltage: 4 kV; nebulizer pressure: 0.3 bar; dry gas flow rate: 3 L/min; dry gas temperature: 120 °C; funnel 1 RF voltage: 400 Vpp; funnel 2 RF voltage: 600 Vpp; hexapole voltage: 800 Vpp; in-source collision-induced dissociation energy: 1 eV; ion energy: 1 eV; low mass filter: m/z = 1000; collision energy: 10 eV; collision RF voltage: 4200 Vpp; transfer time: 130 μs; pre-pulse storage time: 25 μs. The spectra were calibrated using $[Cs(CsI)_n]^+$ clusters as an external reference, generated from a 99% aqueous methanol solution of CsI (0.5 mg/mL) under the same parameters. ^{1}H (400 MHz) and ^{31}P{^{1}H} (162 MHz) NMR charts were recorded on a Jeol JNM-ECS400 spectrometer. All NMR experiments were conducted at 298 K. Chemical shifts in the ^{1}H NMR charts were referenced to the residual proton signal of the solvent (CD_3CN: δ 1.93). Chemical shifts in the ^{31}P{^{1}H} NMR charts were referenced to 85% H_3PO_4 (δ 0.00) as an external standard. Elemental analysis was carried out at the Microanalytical Laboratory, School of Science, The University of Tokyo.

Synthesis of $IrAu_{12}$-R/S·(PF_6)

First, a 200-mL recovery flask equipped with a magnetic stir bar was charged with $(AuCl)_2$((*R*,*R*)-DIPAMP) (162 mg, 175 mmol). CH_2Cl_2 (120 mL) was added to the flask to obtain a colorless solution. Then, $[Ir(COD)Cl]_2$ (14.7 mg, 22 μmol, Au:Ir = 8:1) was added to the solution while stirring to obtain an yellow solution. Finally, a freshly prepared EtOH solution of $NaBH_4$ (16.6 mg in 5 mL, 440 μmol) was added: the color of the solution turned dark brown just after the addition of $NaBH_4$. After stirring for 2 h, the solvent was rotary-evaporated. The dark residue was washed with hexane and then extracted with CH_2Cl_2. After filtration to remove insoluble compounds, the filtrate was evaporated to dryness. EtOH (25 mL) was added to the residue to obtain a dark brown solution. 32.8 μL of 12M HCl aq (1 equiv. to metal atoms) was added to the solution and the solution was stirred for 40 h. The resulting solution was evaporated to dryness, and the dark brown residue was purified by alumina column chromatography using a mixture of CH_2Cl_2 and MeOH (10:1 v/v) as an eluent. Crude Cl-salt of **$IrAu_{12}$-R** was obtained as a brown solid (60 mg, ~12 μmol). The crude product was dissolved into 400 μL of CH_2Cl_2 and diluted with 1.6 mL of MeOH to form a brown solution. To the solution was added a freshly prepared 0.10 M MeOH solution of CAN (60 μL). The color of the solution turned dark green, suggesting the formation of an oxidized from of **$IrAu_{12}$-R** (**$IrAu_{12}$-R^{ox}**). After stirring for 10 min, an addition of a 1 M MeOH solution of $NaPF_6$ formed a green precipitate. The precipitate was collected by centrifugation after stirring for 1h and then washed with EtOH. Green needle crystals of **$IrAu_{12}$-R^{ox}·**$(PF_6)_2$ were obtained by recrystallization from CH_2Cl_2/cyclopentyl methyl ether (CPME) twice. The yield was 25.6 mg (16.8% based on Au). The obtained **$IrAu_{12}$-R^{ox}·**$(PF_6)_2$ (15.6 mg, 3 μmol) was dissolved in a mixture of CH_2Cl_2 and EtOH (3:1, 4 mL). While stirring, a freshly prepared 0.10 M EtOH solution of $NaBH_4$ (80 μL) was added to the solution of **$IrAu_{12}$-R^{ox}** all at once. The color of the solution changed from green to orange after the addition of $NaBH_4$. After stirring for 10 min, the solution was poured into 50 mL of hexane. An orange precipitate of **$IrAu_{12}$-R** was collected by centrifugation and then washed with hexane. Red needle crystals of **$IrAu_{12}$-R·**(PF_6) were obtained by recrystallization from CH_2Cl_2/CPME. The yield was 8.32 mg (54.7% based on **$IrAu_{12}$-R^{ox}·**$(PF_6)_2$). ^{1}H NMR (CD_3CN) δ: 10.20 (d(br), J = 7.33 Hz, 10H), 7.35 (m, 10H), 7.18 (m, 10H), 6.97 (t, J = 7.33 Hz, 10H),

6.76 (d, *J* = 8.24 Hz, 10H) 6.66 –6.57 (m, 40H), 3.57 (s, 30H), 3.19 (s, 6H; CPME). Signals for protons on the ethylene bridge of the DIPAMP ligands were not observed. Anal. Calcd. for $[IrAu_{12}(P_2C_{28}H_{28}O_2)](PF_6)\cdot(C_6H_{12}O)_2$: C, 34.68; H, 3.14; Cl, 1.35. Found: C, 34.45; H, 3.31; Cl, 1.31. The enantiomer **IrAu$_{12}$-S**·(PF_6) was synthesized by the almost same procedures as those of **IrAu$_{12}$-R**·(PF_6) except that $(AuCl)_2$((*S*,*S*)-DIPAMP) was used instead of $(AuCl)_2$((*R*,*R*)-DIPAMP). ^{1}H NMR (CD_3CN) δ: 10.20 (d(br), *J* = 7.33 Hz, 10H), 7.35 (m, 10H), 7.18 (m, 10H), 6.97 (t, *J* = 7.33 Hz, 10H), 6.76 (d, *J* = 8.24 Hz, 10H) 6.66–6.57 (m, 40H), 3.57 (s, 30H), 3.19 (s, 6H; CPME). Signals for protons on the ethylene bridge of the DIPAMP ligands were not observed. Anal. Calcd. for $[IrAu_{12}(P_2C_{28}H_{28}O_2)](PF_6)\cdot(C_6H_{12}O)_2$: C, 34.68; H, 3.14; Cl, 1.35. Found: C, 34.38; H, 3.30; Cl, 1.31.

X-ray crystallography

Single crystals of **IrAu$_{12}$-R/S**·(PF_6) were immersed in Paratone-N oil with the mother liquor to avoid evaporation of the solvent. A suitable crystal for the diffraction experiment was scooped up and rapidly frozen by a cooled N_2 stream. The diffraction experiment for **IrAu$_{12}$-R** was performed on a Bruker D8 VENTURE diffractometer equipped with IμS3.0 microfocus sealed tube, HELIOS multilayer mirror, and PHOTON3 pixel array detector using MoKα radiation. The diffraction experiment for **IrAu$_{12}$-S** was performed on a Rigaku VariMax dual diffractometer with a Pilatus 200K hybrid pixel array detector using CuKα radiation. The data was corrected for Lorentz polarization and absorption correction was done analytically. The initial phase trials were conducted by means of a direct method using SHELXS-2018, and the structures were refined using the full-matrix least-squares method on F^2 by SHELXL-2018.[7] A large solvent accessible void was found in the lattice of each crystal of **IrAu$_{12}$-R/S**, and the solvent molecules inside the void was too disordered to be modeled. Consequently, the diffused electron densities of the crystal were treated by SQUEEZE on the PLATON platform.[8,9] All non-hydrogen atoms were refined anisotropically, and the hydrogen atoms were treated as riding models. The Ir atom was assumed to be located at the center of the M_{13} icosahedron according to the ^{31}P{^{1}H} NMR analysis. CheckCif program generated a B-level alert regarding on negative electron density on Ir atom for **IrAu$_{12}$-R**, while the same level alert regarding on low bond precision for **IrAu$_{12}$-S**. The former is probably due to the incomplete absorption correction of thin needle crystal of **IrAu$_{12}$-R**. The latter is due to the relatively large displacement factor of the ligand shell in **IrAu$_{12}$-S**. Although these alerts are found, the conclusion was not affected since the heavy atom positions are precisely determined. The structure data was deposited at the Cambridge Crystal Structure Center (CCDC) with the depository numbers 2225808 and 2225809 for **IrAu$_{12}$-R/S** respectively.

Results

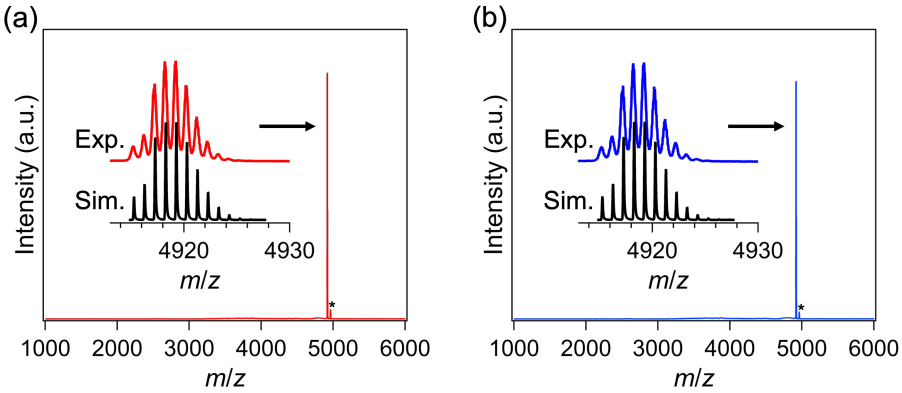

Figure S1. Positive-ion ESI mass spectra of (a) **IrAu$_{12}$-R** and (b) **IrAu$_{12}$-S**. Insets compare the experimental and theoretical isotope patterns. The peaks marked with an asterisk are assigned to [IrAu$_{12}$(DIPAMP)$_5$ClBr]$^+$.

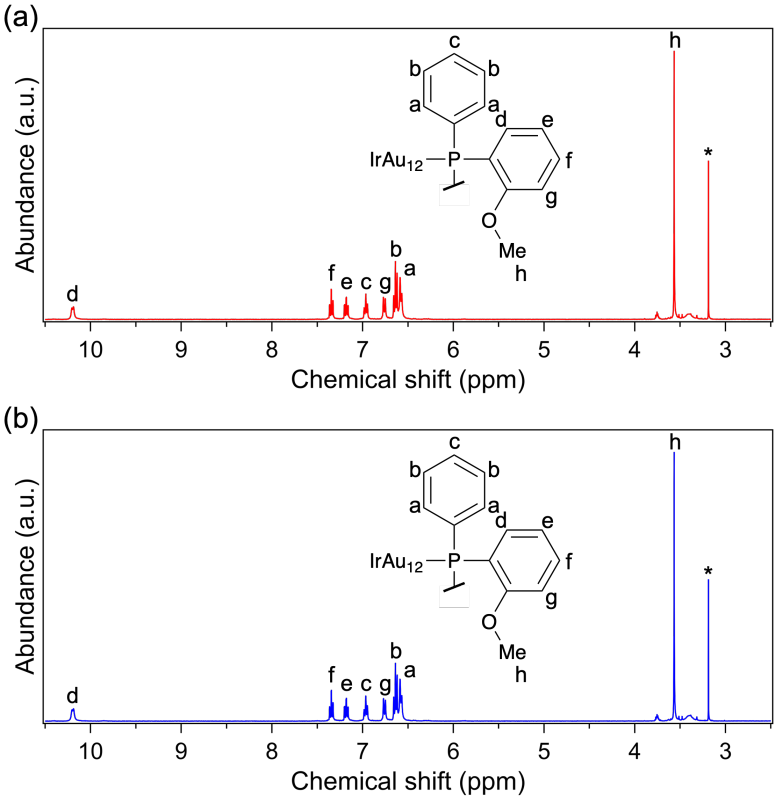

Figure S2. ^{1}H NMR charts of (a) **IrAu$_{12}$-R** and (b) **IrAu$_{12}$-S** in CD_3CN. The peaks marked with an asterisk are assigned to CPME.

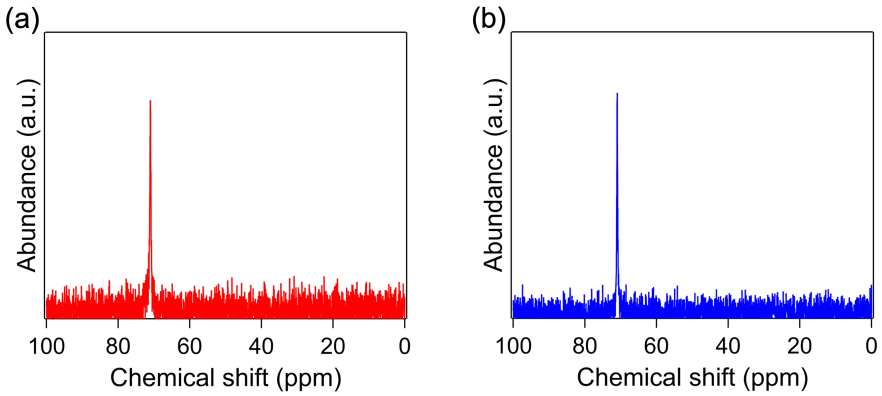

Figure S3. $^{31}P\{^{1}H\}$ NMR chart of (a) **IrAu$_{12}$-R** and (b) **IrAu$_{12}$-S** in CD_3CN.

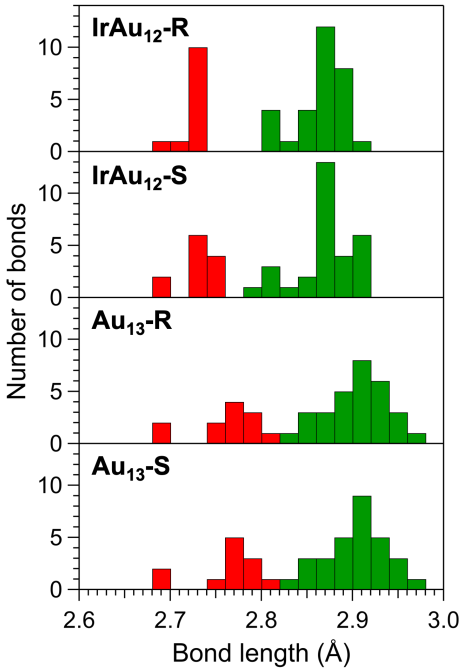

Figure S4. Histograms of the lengths of the metal–metal bonds of **IrAu$_{12}$-R/S** and **Au$_{13}$-R/S**. Red and green bars correspond to the radial M–Au bonds (M = Au, Ir) and lateral Au–Au bonds, respectively.

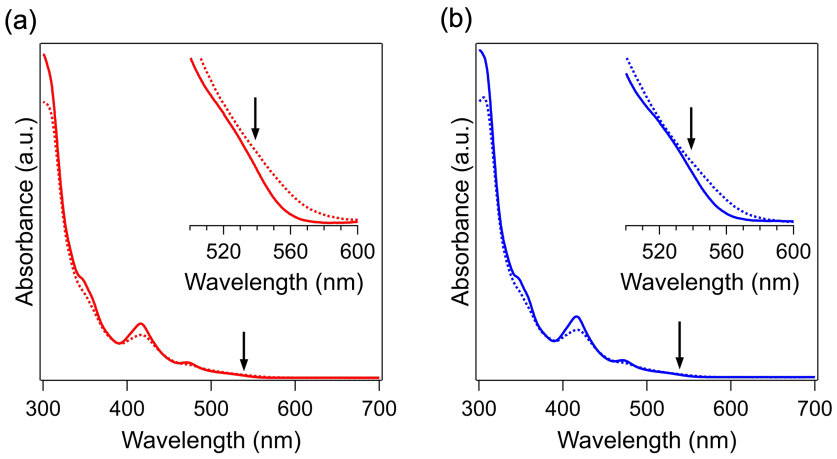

Figure S5. UV–Vis absorption spectra of (a) **IrAu$_{12}$-R** and (b) **IrAu$_{12}$-S** at 300 K (dotted line) and at 200 K (solid line) in MeTHF. The insets show the expanded spectra in the onset region. The arrows indicate the HL gaps estimated from the spectral onset.

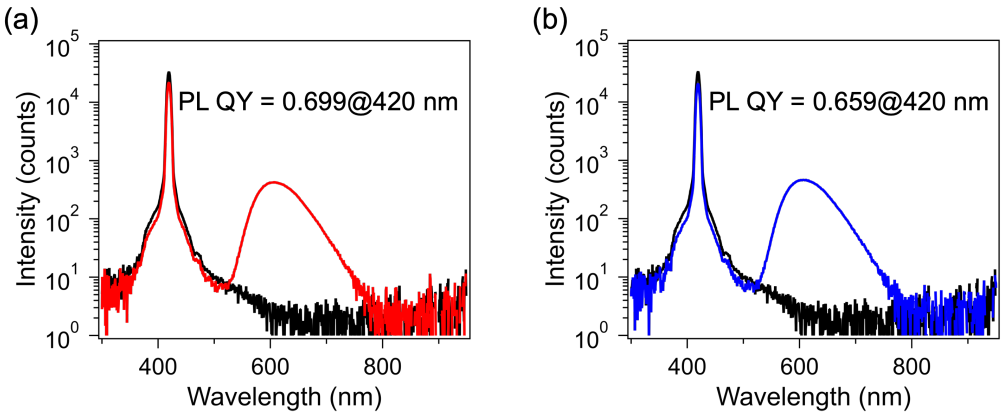

Figure S6. PL emission spectra of (a) **IrAu$_{12}$-R** and (b) **IrAu$_{12}$-S** in deaerated MeTHF for the estimation of PL QY by the absolute method. Black and colored lines correspond to the observed signal without and with samples, respectively.

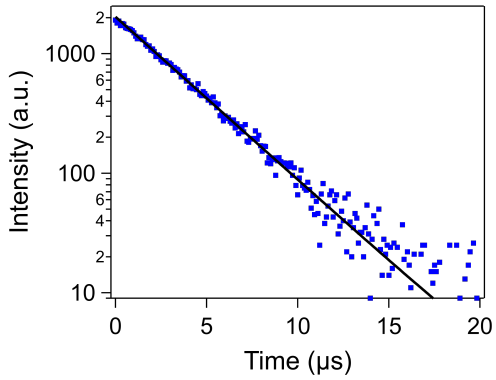

Figure S7. Time-resolve PL decay of **Au$_{13}$-S** probed at 400 nm in MeOH-EtOH mixture (1:1 v/v). The black line represents the fitting result.

Table S1. Average metal-metal bond lengths of **$IrAu_{12}$-R/S** and **Au_{13}-R/S**.

Superatom	Radial bond length (Å)	Lateral bond length (Å)	Total bond length (Å)
$IrAu_{12}$-R	2.726(12)	2.866(26)	2.826(68)
$IrAu_{12}$-S	2.729(17)	2.870(34)	2.830(70)
Au_{13}-R	2.761(33)	2.904(30)	2.863(72)
Au_{13}-S	2.761(34)	2.903(32)	2.863(72)

Table S2. Crystal data.

	$IrAu_{12}$-R	**$IrAu_{12}$-S**
Formula	$C_{140}H_{140}Au_{12}Cl_2F_6IrO_{10}P_{11}$	$C_{146}H_{152}Au_{12}Cl_2F_6IrO_{11}P_{11}$
FW (g mol^{-1})	5063.88	5164.04
Crystal size (mm)	0.216 × 0.034 × 0.027	0.139 × 0.033 × 0.022
Crystal system	Orthorhombic	Orthorhombic
Space group, Z	$P2_12_12_1$, 4	$P2_12_12_1$, 4
a (Å)	20.2131(9)	18.7320(3)
b (Å)	23.6071(12)	28.9403(3)
c (Å)	33.7333(17)	30.8548(3)
V (Å^3)	16096.6(14)	16726.7(3)
T (K)	100.0(5)	93(2)
ρ_{calc} (g cm^{-3})	2.090	2.051
μ (mm^{-1})	11.911	22.454
θ range (°)	2.2450 – 25.3077	3.0370 – 69.8740
Measured reflections	173675	100017
Unique reflections	29526 (R_{int} = 0.0829)	30593 (R_{int} = 0.0632)
Data/restraints/parameters	29526/1827/1400	30593/1573/1583
$R^{a,b}$ indices [$I > 2\sigma(I)$]	R_1 = 0.0476, wR_2 = 0.1032	R_1 = 0.0517, wR_2 = 0.1351
$R^{a,b}$ indices [all data]	R_1 = 0.0548, wR_2 = 0.1058	R_1 = 0.0639, wR_2 = 0.1434
Goodness-of-fit on F^2	1.126	1.004
Flack parameter	0.060(11)	-0.005(8)

[a] $R_1 = \Sigma(||F_o| - |F_c||)/\Sigma|F_o|$. [b] $wR_2 = [\Sigma[w(F_o^2 - F_c^2)^2]/\Sigma[w(F_o^2)^2]]^{1/2}$, $w = 1/[\sigma^2(F_o^2) + (ap)^2 + bp]$, where $p = [\max(F_o^2, 0) + 2F_c^2]/3$.

References

(1) Leyva-Pérez, A.; Doménech-Carbó, A.; Corma, A. Unique Distal Size Selectivity with a Digold Catalyst during Alkyne Homocoupling. *Nat. Commun.* **2015**, *6*, 6703.

(2) Brandys, M.-C.; Jennings, M. C.; Puddephatt, R. J. Luminescent Gold(I) Macrocycles with Diphosphine and 4,4'-Bipyrydyl Ligands. *J. Chem. Soc., Dalton Trans.* **2000**, 4601‑4606.

(3) Shichibu, Y.; Ogawa, Y.; Sugiuchi, M.; Konishi, K. Chiroptical Activity of Au_{13} Clusters: Experimental and Theoretical Understanding of the Origin of Helical Charge Movements. *Nanoscale Adv.* **2021**, *3*, 1005–1011.

(4) Herde, J. L.; Lambert, J. C.; Senoff, C. V. Cyclooctene and 1,5-Cyclooctadiene Complexes of Iridium(I). *Inorg. Synth.* **1974**, *15*, 18–20.

(5) Shichibu, Y.; Konishi, K. HCl-Induced Nuclearity Convergence in Diphosphine-Protected Ultrasmall Gold Clusters: A Novel Synthetic Route to "Magic-Number" Au_{13} Clusters. *Small* **2010**, *6*, 1216–1220.

(6) Hirai, H.; Takano, S.; Nakamura, T.; Tsukuda, T. Understanding Doping Effects on Electronic Structures of Gold Superatoms: A case Study of Diphosphine-Protected $M@Au_{12}$ (M = Au, Pt, Ir). *Inorg. Chem.* **2020**, *59*, 17889–17895.

(7) Sheldrick, G. M. Crystal Structure Refinement with *SHELXL*. *Acta Cryst. C* **2015**, *71*, 3–8.

(8) Van der Sluis, P.; Spek, A. L. BYPASS: an Effective Method for the Refinement of Crystal Structures Containing Disordered Solvent Regions. *Acta Cryst. A* **1990**, *46*, 194–201.

(9) Spek, A. L. Single-Crystal Structure Validation with the Program *PLATON*. *J. Appl. Cryst.* **2003**, *36*, 7–13.